Ocean pH time-series and drivers of variability along the northern Channel Islands, California, USA

Lydia Kapsenberg[†]* Gretchen E. Hofmann
Department of Ecology, Evolution and Marine Biology, University of California Santa Barbara, Santa Barbara, California

Abstract

Eastern boundary current systems (EBCSs) experience dynamic fluctuations in seawater pH due to coastal upwelling and primary production. The lack of high-resolution pH observations in EBCSs limits the ability to relate field pH exposures to performance of coastal marine species under future ocean change (acidification, warming). This 3-yr study describes spatio-temporal pH variability across the northern Channel Islands, along a persistent temperature gradient (1–4°C) within the eastern boundary California Current System. pH and Conductivity, Temperature, Depth, and Oxygen sensors were deployed on island piers in eelgrass and kelp habitat and on a subtidal mooring. Due to event-scale primary production, the temperature gradient across the islands did not manifest in a pH gradient. We resolved spatial pH variability on diel (ΔpH_T 0.05–0.2: photosynthesis), event-scale (ΔpH_T <0.1–0.2: upwelling, phytoplankton blooms, wind relaxation), and seasonal (ΔpH_T 0.06: warming) time frames. In the kelp forest, summer mean pH_T (8.01–8.02) and magnitude of diel pH_T cycles (ΔpH_T 0.12–0.10) were comparable year-to-year, despite 2.1°C warming from 2012 to 2014. Compared to nearby mainland sites, the northern Channel Islands experienced few low pH events. The majority of pH_T observations were >7.9. The lowest pH observations (>1 SD below mean pH_T) occurred under either warm (respiration during warm nights) or cold (advection of upwelled water) temperatures. We emphasize the importance of incorporating site-specific environmental variability in studies of ocean change biology, particularly in the design of multistressor experiments.

Coastal marine ecosystems are complex environments with spatio-temporal variability in productivity and bulk water mass movement. Physical and biological processes give rise to spatially unique pH-seascapes and are expected to change with climate change (Hofmann et al. 2011; Hauri et al. 2013; Hoegh-Guldberg et al. 2014; Takeshita et al. 2015). Particularly, eastern boundary current systems (EBCSs) are predicted to be one of the first coastal ecosystems to cross thresholds of ocean acidification due to coastal upwelling (Gruber et al. 2012). While upwelling is a natural phenomenon, the associated onshore delivery of low pH water is exacerbated by ocean acidification (Feely et al. 2008).

The heightened sensitivity of EBCSs to ocean change has already been realized in economic losses of shellfish production (Barton et al. 2012). The intensity of winds that are favorable to upwelling has increased in EBCSs (Sydeman et al. 2014) and upwelling events are predicted to increase in duration and strength with future climate change (Wang et al. 2015). As upwelling replenishes surface waters with nutrients yielding phytoplankton blooms that draw pCO_2 down to below atmospheric equilibrium (Hales et al. 2005), changes in upwelling may also alter coastal pH variability through influences on primary production in the future. Our understanding of present-day patterns in coastal carbon chemistry is often underdescribed making it challenging to predict which coastal zones will be resistant or vulnerable to the effects of ocean change. In an effort to increase the knowledge base on coastal pH variability in an EBCS, we examined pH heterogeneity across a small geographic scale and link patterns to local and regional processes that are relevant for marine species and coastal management.

As an EBCS with strong seasonal upwelling, the California Current System (CCS), extending from southern British Columbia to Baja California, is extremely vulnerable to the effects of ocean acidification (Feely et al. 2008; Gruber et al. 2012; Hauri

*Correspondence: lydia.kapsenberg@obs-vlfr.fr

[†]Present address: Sorbonne Universités, Université Pierre et Marie Curie-Paris 6, CNRS-INSU, Laboratoire d'Océanographie de Villefranche, France

Additional Supporting Information may be found in the online version of this article.

et al. 2013). Summertime upwelling contributes to seasonal and spatial pH variability in the CCS (Hauri et al. 2013). Individual upwelling events have increased in duration and intensity from 1967 to 2010 (Iles et al. 2012). Both field data and model simulations of future conditions show that near-shore pH is lower than offshore surface waters (Feely et al. 2008; Gruber et al. 2012). Thus the vulnerability to ocean acidification lies in coastal habitats. Near-shore (50 km) CCS waters already exhibit pH levels outside of preindustrial conditions, and a complete departure from the present-day pH variability envelope is predicted to occur as early as 2040 (Hauri et al. 2013). While incorporating seasonal pH changes helps refine predictive models, extensive documentation of event-scale to short-term pH variability is lacking, making model predictions uncertain in relation to species' future exposures.

The scarcity of time-series pH data,* to inform experiments, hampers the understanding of organismal pH tolerance and adaptation. Observations from autonomous pH sensors document patterns of natural pH variability in coastal ecosystems that often meet or exceed the magnitude of predicted global ocean acidification (Hofmann et al. 2011). Use of high-resolution, autonomously-collected environmental data provides a major advantage over manual sampling through the ability to identify short-term cycles and onset of events (e.g., Frieder et al. 2012). Such data are necessary to link habitat seawater chemistry to organismal pH tolerance (e.g., Yu et al. 2011; Price et al. 2012; Frieder et al. 2014; Kapsenberg and Hofmann 2014) and extend our understanding of future coastal ocean pH variability (Takeshita et al. 2015) and ocean acidification trends (Keller et al. 2014). For biological experiments conducted on species in the CCS, treatments designed to mimic future pH conditions often did not extend outside the range of the species' estimated present-day pH (pCO$_2$) exposure (Reum et al. 2015). Moreover, a handful of such laboratory experiments revealed negative effects of present-day conditions (Reum et al. 2015), which have also been observed in the wild and in aquaculture production (Barton et al. 2012; Bednaršek et al. 2014). Although there is evidence that some species have the potential to adapt to changing pH (e.g., Kelly et al. 2013; Pespeni et al. 2013; Malvezzi et al. 2015), these efforts are in their infancy and require detailed knowledge of environmental pH exposures. Therefore, we provide such environmental data and document pH variability in a sub-region of the CCS.

One distinctive geographic feature in the CCS is the Santa Barbara Channel (SBC), located in the Southern California Bight (Fig. 1). The SBC is formed by a ~90° turn in the coast-
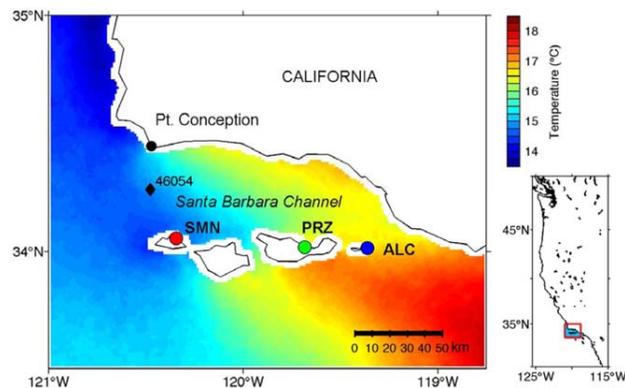
Fig. 1. Three-year (2012–2014) sea surface temperature composite of the Santa Barbara Channel region. Study sites are noted on San Miguel Island north mooring (SMN, red circle), Prisoner's Harbor pier on Santa Cruz Island (PRZ, green circle), and Anacapa Island Landing Cove pier (ALC, blue circle). Composite represents means for cloud-free pixels using daily satellite images. Diamond indicates National Data Buoy Center station 46054.

line at Pt. Conception and bound by the four northern Channel Islands (San Miguel, Santa Rosa, Santa Cruz, and Anacapa). The islands are part of the Channel Islands National Park and National Marine Sanctuary. Across the SBC, multiple abiotic gradients are established due to the nearly-persistent cyclonic flow, unique bathymetry and east–west orientation of the channel (Harms and Winant 1998). For example, Pt. Conception creates a wind shadow such that both wind and current strength decrease from west to east along the islands (Harms and Winant 1998; Dorman and Winant 2000). During upwelling-favorable wind stress, equatorward flow north of Pt. Conception extends along the islands (Harms and Winant 1998). Given the stronger winds, currents, and cooler temperatures at San Miguel Island, the pH signatures of upwelled waters may manifest as well. As part of this study, we test the hypothesis that pH increases from west to east along the coastline of the Channel Islands following a gradient in temperature and upwelling (Harms and Winant 1998). Identification of persistent pH gradients across a species' biogeographic range could aid studies of local pH adaptation and acclimatization (Hofmann et al. 2014). In this effort, we quantify pH variability along the northern Channel Islands and link observations to local and regional scale physical and biological drivers.

Materials and procedures

Study region

Located in the Southern California Bight, the SBC is ~100 km long and 40 km wide with a central basin depth of 500 m, a sill at both the eastern (220 m) and western (430 m) entrance and shallow connections between the islands (~40 m; Harms and Winant 1998). In the Bight, equatorward flow is influenced by the California Current (cold, near-surface,

200–300 km offshore) and coastal poleward flow is facilitated by the Southern California Counter Current (warm, high salinity, flow over the continental shelf is strongest in the fall and winter) and the California Undercurrent (deep flow along the continental slope; Lynn and Simpson 1987; Dong et al. 2009). In the SBC, these dynamics result in flow that is generally east–west along the mainland and west–east along the islands and generate a nearly persistent cyclonic flow within the SBC (Harms and Winant 1998; Dong et al. 2009).

The physical characteristics of the SBC result in multiple abiotic gradients across the Channel Islands. A persistent temperature difference of 1–4°C is maintained between San Miguel Island and Anacapa Island (Harms and Winant 1998), with a front that oscillates along the center coastline of Santa Cruz Island (Selkoe et al. 2006). Coastal upwelling north of Pt. Conception yields cool temperatures in the west and poleward flow brings in warm water in from the east (Harms and Winant 1998; Lagerloef and Bernstein 1988; Otero and Siegel 2004). In addition, wind and current strength decrease from west to east (Harms and Winant 1998; Dorman and Winant 2000).

Sites and sensor deployments

To test the hypothesis that abiotic environmental gradients establish a pH gradient, we quantified pH variability on different temporal and spatial scales. SeaFET pH sensors (Martz et al. 2010) and Conductivity, Temperature, Depth, and Oxygen sensors (CTDO sensors, Sea-Bird Electronics 37-SMP-ODO Micro-CAT C-T-ODO (P) Recorder) were deployed at three sites along the northern Channel Islands: (1) Anacapa Island Landing Cove pier (ALC, 34°00.985′N, 119°21.724′W) in a marine reserve with kelp forest habitat, (2) Santa Cruz Island Prisoner's Harbor pier (PRZ, 34°01.225′N, 119°41.057′W) surrounded by a large shallow eelgrass bed (*Zostera pacifica*), and (3) San Miguel Island northern subtidal mooring (SMN, 34°03.417′N, 120°20.731′W) at 6 m in open water over a sandy bottom at 18 m depth (Fig. 1). Sensors at ALC and PRZ were deployed at 3–4 m depth and <1 m from the benthos on a pier piling. For reference, ALC and PRZ represent environmental conditions relevant to benthic marine invertebrates whereas SMN reflects environmental conditions relevant to pelagic life stages such as free-swimming invertebrate larvae. pH sensors were first deployed in 2012 at ALC and PRZ and recorded pH and temperature every 30 min for 10 s reading periods. pH sensors were not pumped. In May 2013, CTDO sensors were deployed in addition to pH sensors at ALC and PRZ. CTDO sensors were actively pumped through an antifouling passage and temperature, salinity, pressure, and dissolved oxygen were recorded every 15 min. In August 2013, the sensor array from PRZ was moved to SMN for a 1-yr overlapping period of data collection with ALC. During this time a pH sensor was intermittently deployed at PRZ. At each site sensors were swapped every 2–3 months. SeaFET sensor surfaces did not exhibit biofouling on recoveries. Following the last CTDO sensor deployments in September 2014, sampling frequency on pH sensors was increased to 20 min. Following linear interpolation when necessary, all data are reported on a 30 min frequency.

Data processing

Calibration samples for SeaFET sensors were collected 1–8 times during each deployment via SCUBA, free diving, or a GO-FLOW (General Oceanics) bottle drop from the pier following Standard Operating Procedures (SOP) 1 (Dickson et al. 2007). Samples were fixed immediately with saturated mercuric chloride. Water samples were analyzed for $pH_{25°C}$ (spectrophotometric method, SOB 6b, Dickson et al. 2007; using m-cresol purple from Sigma-Aldrich®) and total alkalinity (A_T, SOP 3b, Dickson et al. 2007; using open-cell titrator Mettler-Toledo T50). Salinity (YSI 3100 Conductivity Instrument) was measured when no corresponding salinity measurements were available from a CTDO sensor. In situ pH_T (total hydrogen ion scale) were calculated (CO2Calc, Robbins et al. 2010) using either temperature recorded by the SeaFET or CTDO sensor, when available, and using CO_2 constants from Mehrbach et al. (1973) refit by Dickson and Millero (1987). All pH data are reported as pH_T.

SeaFET data processing followed methods from Bresnahan et al. (2014) for single and multiple calibration samples, using Matlab (R2012b). When SeaFET pH sensor deployments were paired with CTDO sensors (May 2013–September 2014), temperature data from the CTDO sensors were used to correct for the offset associated with the uncalibrated SeaFET thermistor. CTDO sensors underwent factory calibration at the start and end of the project. Between deployments, sensors were rinsed with DI water and dilute Triton-X. CTDO data were interpolated onto the Sea-FET sampling period and all data were reported in Coordinated Universal Time, unless specified otherwise. For one 24-h gap, CTDO data were interpolated to match the deployment length of the pH sensor at ALC when necessary for computations. Rare low pH observations, where pH declined to below pH 7.7 within two observations and independent of changes in temperature, were removed for quality control. Oxygen saturation data, recorded by the CTDO sensor, were converted to dissolved oxygen (DO, μmol kg^{-1}), using the oxygen solubility combined fit conversion equation from García and Gordon (1992).

Due to the lack of salinity data throughout the 3-yr study period, we only provide estimated aragonite saturation state (Ω_{arag}) and pCO_2 calculations for the period during which CTDO sensors were deployed at SMN and ALC. A_T time-series were predicted ($A_{T\ pred}$) using an established relationship of A_T with observed sea surface salinity (SSS_o) and temperature (SST_o), for Equatorial Upwelling regions as described by Lee et al. (2006), where SSS_o and SST_o were recorded by CTDO sensors at each site:

$$A_{T\ pred} = 2294 + 64.88 \times (SSS_o - 35) + 0.39 \times (SSS_o - 35)^2 - \\ 4.52 \times (SST_o - 29) - 0.232 \times (SST_o - 29)^2 \tag{1}$$

$A_{T\ pred}$ was corrected ($A_{T\ corr}$) for observed offsets from measured A_T on calibration samples compared to $A_{T\ pred}$;

offsets were calculated at each sample point and mean offset was used to adjust the A_T time-series. Aragonite saturation state and pCO_2 were calculated using CO2SYS for Matlab (van Heuven et al. 2011) and CO_2 constants from Mehrbach et al. (1973) refit by Dickson and Millero (1987). In addition to Ω_{arag} and pCO_2, total dissolved inorganic carbon (DIC) time-series were calculated and included in the online publication of this dataset, along with pH, CTDO and $A_{T\ corr}$.

Data analysis

Data were analyzed in raw form, as monthly means, and following a 48-h high-pass filter to remove seasonal and event-scale signals or low-pass filter to remove diel cycles. The maximum daily ranges of pH observations within a 24-h period were calculated using 48-h high-pass filtered data and reported as "diel pH cycles" (i.e., twice the amplitude). To investigate pH variability independent of temperature effects on pH, pH_T was normalized to 16°C ($pH_{T\ N16°C}$). Comparisons between SMN and ALC were made using data from exactly 1 yr: 20 August 2013 to 20 August 2014. This same date range was used to calculate anomalies, where the site-specific mean from 20 August 2013 to 20 August 2014 was subtracted from the time-series (pH, oxygen, temperature, salinity). Ranges in pH_T were reported from 0.5^{th} to 99.5^{th} percentiles. Low pH events were investigated in relation to temperature.

To identify potential regional drivers of the observed pH variability along the northern Channel Islands, observations of regional sea surface temperature (SST, °C), Chlorophyll *a* concentrations (Chl *a*, mg m^{-3}), and wind stress were investigated. Satellite-derived daily SST and Chl *a* images for the SBC region were downloaded from the Scripps Photobiology Group (http://spg.ucsd.edu/Satellite_Data/California_Current/, Kahru et al. 2012) and processed for composite SST and Chl *a* maps during periods of positive and negative pH anomalies. For a given time interval, all cloud-free pixels were averaged across daily images. As a guideline, Chl *a* threshold indicating a phytoplankton bloom was considered to be ≥ 2 mg m^{-3} (Otero and Siegel 2004). Time-series pH data were divided into phases with corresponding SST and Chl *a* maps and CTDO observations to highlight drivers of pH variability. Wind data were downloaded from the National Data Buoy Center buoy 46054 (http://www.ndbc.noaa.gov/), located at the western end of the SBC, and rotated onto its principle axes (Fig. 1). Positive wind stress denotes alongshore equatorward winds. All analyses were performed in Matlab (R2012b).

Error estimates

Errors in pH_T measurements of field samples are largely due to the use of unpurified m-cresol dye (0.02, Liu et al. 2011), user error (±0.006, Kapsenberg et al. 2015) and spatio-temporal mismatch of the calibration samples (±0.010 for SMN, ±0.026 for PRZ, ±0.005 for ALC). Spatio-temporal mismatch error was calculated as the absolute mean offset of discrete samples from sensor observations for deployments with >1 discrete calibration sample (Fig. 2). The resultant estimated standard uncertainty of pH data presented here differed by site and was ±0.023 (SMN), ±0.033 (PRZ), and ±0.022 (ALC). The error in pH due to the use of uncalibrated SeaFET thermistors (deployments February 2012–May 2013, September 2014–May 2015) was ±0.005 and did not impact the estimated standard uncertainty. The accuracy of field samples is less than the resolution of SeaFET pH sensors (0.001) and pH is reported to a precision of 0.01.

Post calibration of CTDO sensors revealed negligible drifts in oxygen, salinity, and temperature. A total of six in situ water samples were collected for Winkler determination for dissolved oxygen (Wetzel and Likens 1991) and showed a mean $0.9\% \pm 0.9\%$ positive offset from sensor observations (maximum offset was 2.4%, see Supporting Information 1). Post calibration indicated oxygen sensor drift of <1–2% across the three instruments. The data were not corrected for drift of the oxygen sensor and accuracy for this data is ±2%. A small drift in conductivity resulted in a salinity accuracy of ±0.02. Temperature drift was <0.001°C for all sensors with a reported accuracy of ±0.002°C. Data were not corrected for sensor drift.

Results

Spatial range in pH observations

The data collected across the islands from February 2012 to May 2015 varied on temporal and spatial scales (for complete time-series; see Supporting Information 2). Patterns in pH variability were detected on diel, event, and seasonal time scales, with limited interannual variability. For all data collected, mean pH_T (±SD) at each site was: SMN 8.05 ± 0.05, PRZ 8.00 ± 0.06, and ALC 8.01 ± 0.04. At each site, 99% of pH_T observations fell between 7.92–8.16, 7.81–8.16, and 7.88–8.12, at SMN, PRZ and ALC, respectively. PRZ exhibited the widest range in pH_T observations of 0.36. SMN and ALC had a pH_T range of 0.24. For periods <48-h, the range in pH_T observations was reduced to 0.27 at PRZ and to 0.21 at SMN and ALC, respectively (Fig. 3). Time-series $A_{T\ corr}$, Ω_{arag} and pCO_2 are described in Supporting Information 3.

During the overlapping deployment period at ALC and SMN (20 August 2013–20 August 2014), SMN exhibited a greater range in pH_T (0.24) and higher mean pH_T (8.05 ± 0.05) compared to ALC (8.02 ± 0.03), which exhibited a pH_T range of 0.18. These differences were due to distinct positive and negative event-scale (days to weeks) pH anomalies observed at SMN and do not support the hypothesis of a persistent pH gradient across the northern Channel Islands.

Diel pH cycles

Significant 24-h periodicities in pH were observed at all sites (Supporting Information 4). The magnitude of diel pH cycles (twice the amplitude) were investigated following 48-h high-pass filtering to remove event-scale and seasonal signatures (Fig. 4). In general, diel pH cycles at PRZ were larger
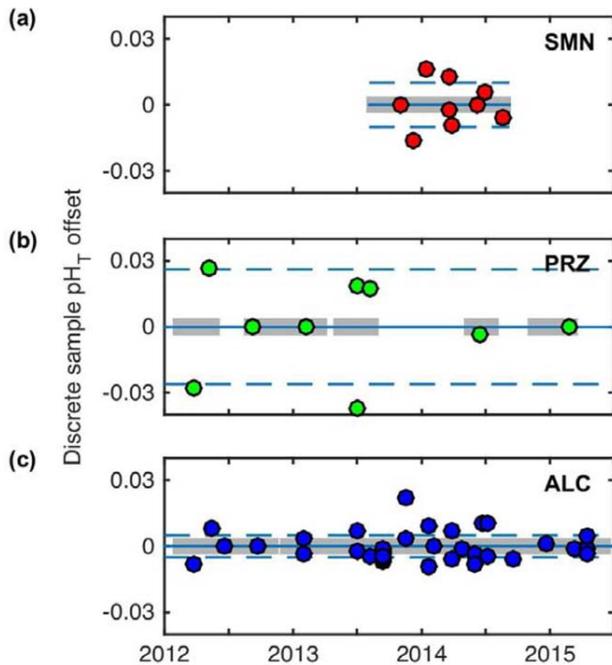
Fig. 2. Offset in pH of discrete calibration samples compared to SeaFET pH sensor data collected at SMN (a), PRZ (b), and ALC (c). Grey blocks represent sensor deployment periods. Dashed lines represent the reported error in pH measurements associated with spatio-temporal mismatch of sampling only. The displayed discrete samples were used to calculate the sensor data (solid reference line = 0). Deployments with one calibration sample show an offset of 0 and were not incorporated in the spatio-temporal mismatch error calculation. Calibration samples from the last two deployments at PRZ were not equal to zero as the sensor data was interpolated onto a time stamp that differed from the original sampling frequency; these offsets were not incorporated into error calculation for PRZ.

and more variable than the other two sites, despite the fact that ALC and PRZ experienced similar thermal regimes (Supporting Information 2). Peaks in the daily magnitude of pH change occurred at different times in the year at each site. Magnitude of diel pH cycles peaked in spring, summer, and spring and fall, for PRZ (eelgrass), ALC (kelp forest), and SMN (open water), respectively. High-pass filtered oxygen and pH observations were positively correlated at all sites, with a stronger correlation at vegetated sites, ALC ($R^2 = 0.91$, $F = 234{,}156$, $p < 0.001$, $n = 23{,}660$) and PRZ ($R^2 = 0.86$, $F = 2.3378$, $p < 0.001$, $n = 3637$), compared to SMN ($R^2 = 0.79$, $F = 64{,}182$, $p < 0.001$, $n = 17{,}437$).

PRZ exhibited the largest seasonal change in diel pH_T cycles where cycles in April (0.20) were approximately tripled from November and December observations (0.07, 0.06). The largest diel pH cycles at PRZ occurred during months of lowest temperature and lowest mean pH (March, April). When comparing the vegetated sites, monthly mean diel pH cycles were always larger at PRZ compared to ALC.

ALC exhibited a seasonal increase in magnitude of diel pH_T cycles from, on average, 0.05 in winter to 0.10 in summer. At SMN, the magnitude of diel pH_T cycles peaked once in October (0.09) and again in May (0.11), which reflected an approximate doubling of diel pH cycles observed in winter and early spring despite being outside of vegetated habitat.

Event-scale variability

Event-scale pH anomalies were investigated and compared for SMN and ALC for the overlapping period of paired pH and CTDO sensor deployments. Three event-scale effects were observed and were most apparent at SMN: (1) phytoplankton blooms (0.1–0.2 pH_T increase), (2) advection of upwelled water (0.1 pH_T decrease), and (3) wind relaxation (increased high-frequency, <1 d, pH_T variability). To describe event-scale variability, pH time-series data were divided into distinct phases and investigated alongside corresponding SST and Chl *a* maps.

The first example describes a regionally restricted *phytoplankton bloom* that occurred during disparate pH anomalies at SMN and ALC. Here, a near-persistent positive pH and oxygen anomaly at SMN occurred from August to mid-October in 2013, but not at ALC (Fig. 5, Phase I). During this anomaly, pH and oxygen oscillated above annual means and exhibited similar patterns in variability. This event coincided with persistent observations of Chl *a* concentrations indicative of phytoplankton blooms (Fig. 5c). The bloom subsided in the latter half of October into December at the same time that pH and oxygen returned to nonanomalous conditions at SMN (Fig. 5, Phase II). In addition, diel pH cycles at SMN were larger during Phase I (September, October) compared to those observed during Phase II (November, December) once the bloom had subsided (Fig. 4). The phytoplankton bloom was restricted to the western end of the SBC, surrounding San Miguel Island but not Anacapa Island. Throughout Phase I and II, pH remained slightly negatively anomalous at ALC.

A second example of event-scale variability was identified during the upwelling season. The largest variability in event-scale pH was observed during April and May at SMN. During these months, pH exhibited a mostly negative anomaly, due to *advection of upwelled water* with high salinity and low oxygen and temperature, which was interrupted by pH increases, due to phytoplankton blooms (Fig. 6). For Fig. 6, we focused on describing pH variability at SMN and compared patterns observed at ALC.

At the start of the upwelling season in April, an initial pH_T increase of ~0.15 at SMN occurred on 02 April 2014 at the same time as an increase in regional Chl *a* (Fig. 6, Phase I). These conditions persisted for 10 d and corresponded to a positive oxygen anomaly during which temperature declined and salinity increased (i.e., intrusion of an upwelled water mass). Next, pH_T declined (~0.12) over the following 26 d (Fig. 6, Phase II). This phase marked the lowest pH and temperature and highest salinity observations at SMN. SST
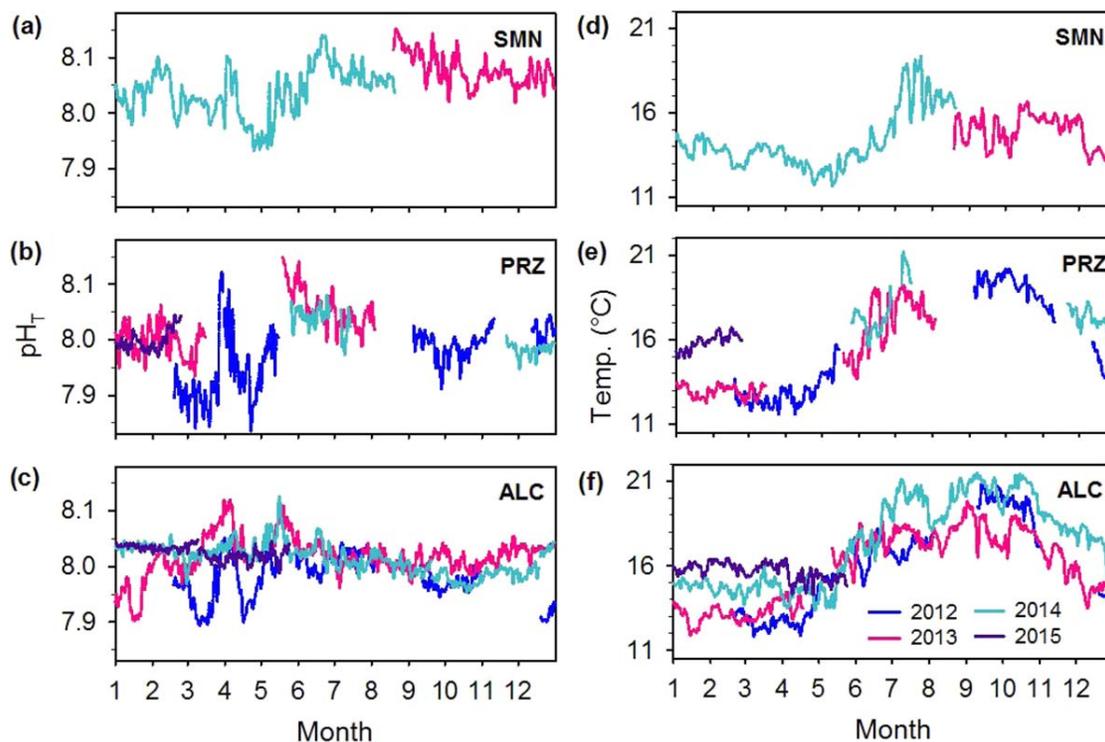
Fig. 3. Time-series of 48-h low-pass filtered pH (a–c) and temperature (d–f) by site. Colors represent different years. Site codes are the same as in Fig. 1.

composites during Phase II suggest that these water masses were advected to SMN from upwelling events north of Pt. Conception. During the presence of these upwelled waters, a 1-d pH_T increase (0.15) occurred with the overnight appearance of high levels of regional Chl *a* (Fig. 6, Phase III). With strengthening equatorward winds, pH_T decreased by 0.15 and remained low for 2 d, despite a continued increase in regional Chl *a*. This marked the end of the low pH conditions in spring at SMN. Next, pH recovered to a small positive anomaly during wind relaxation (details discussed below) and intrusion of warm, low salinity water from the south (Fig. 6, Phase IV). This warm water intrusion was observable at both SMN and ALC in the time-series data and SST plots.

Overall, during the period of the largest pH variability at SMN, April and May, ALC generally exhibited a positive pH and oxygen anomaly following the first channel-wide Chl *a* increase on 02 April 2014 (Fig. 6, Phase I). pH and oxygen anomalies roughly returned to a nonanomalous state at ALC at the same time as (1) seasonal warming (which could partially account for a decrease in pH) and (2) the near-disappearance of Chl *a* in the SBC (Fig. 6, Phase V). Along with the disparate pH and oxygen anomalies observed between SMN and ALC in the fall (Fig. 5), these results highlight Anacapa Island's isolation from regional processes that operate at the western end of the SBC leading to reduced pH variability at ALC compared to SMN.

The 3rd event-scale variability that was identified was related to wind stress. Due to the gradient of wind stress in the SBC (Harms and Winant 1998), wind effects were most apparent at SMN. Throughout the study period, wind relaxation events corresponded with periods of *increased high-frequency pH variability*, or, alternatively, high wind stress diminished high-frequency pH variability. This effect was observable in January; a period of relatively low pH variability (Fig. 7a–e). Here, high wind stress corresponded with decreasing pH, oxygen, temperature and increasing salinity, signifying intrusion of upwelled water. During spring and a period of relatively high pH variability (Fig. 7f–j), wind relaxation in May occurred with increasing pH, oxygen, temperature and decreasing salinity. In both examples, wind relaxation corresponded with an increase in high-frequency pH, oxygen, temperature, and salinity variability. As wind stress increased, these high frequencies diminished with a 1-d delayed effect. This suggests that periods of high wind stress mask the effect of processes that induce high-frequency pH variability.

It is noteworthy that event-scale pH variability was observed at all island sites, for example, at PRZ and ALC in March and April 2012 (Fig. 3). While we lack CTDO data for that deployment period, the 0.15–0.20 pH_T increase over 10 d occurred with the appearance of Chl *a* near the island coastlines (Chl *a* composite not shown). Following a decline in pH at the same time as a reduction in Chl *a*, pH_T
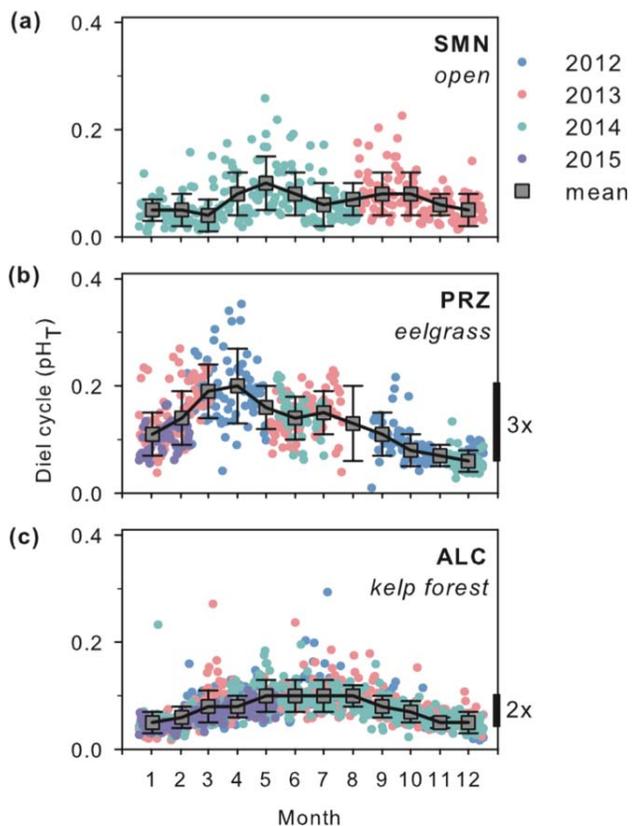
Fig. 4. Seasonal evolution of diel pH cycles in open water (a, SMN), an eelgrass bed (b, PRZ) and kelp forest (c, ALC). Seasonal tripling (b) and doubling (c) of diel pH cycles are shown on the right *y*-axis. Diel cycles were calculated following 48-h high-pass filtering. Daily observations are colored by year. Squares denote combined-year monthly means ± SD. Site codes are the same as in Fig. 1.

increased again by 0.1 at both sites with a second and larger increase in regional Chl *a* that was accompanied by ~4°C temperature increase.

Seasonal trends

Evidence for a seasonal pH cycle was found across the islands (Table 1). ALC and PRZ appeared to share a similar trend in seasonal pH_T change of 0.06–0.08. At ALC, peak pH_T occurred in May (8.04 ± 0.03) and declined to October (7.98 ± 0.02). At PRZ, peak pH_T occurred in June (8.06 ± 0.02) and declined to October (7.98 ± 0.02). As a caveat, data collection was not continuous at PRZ and low monthly mean pH in March and April was biased by two low pH events in 2012, which were also observed at ALC (Fig. 3a–c). The seasonal cycle at SMN was described over 1 yr and exhibited a different trend from ALC and PRZ. At SMN, pH_T generally declined from August (8.08 ± 0.04) through April and peaked in summer immediately following months of low pH_T (8.00 in April, May).

Interannual comparisons

Interannual comparisons of pH were made using data from ALC, as this was the most complete data record over the 3 yr study period. At ALC, mean pH_T (±SD) for data collected from 2012 to 2014 was 7.98 ± 0.05, 8.02 ± 0.04, and 8.01 ± 0.04, respectively. Event-scale variability observed in winter and spring (e.g., 2012, 2013), contrasts the stability of summer pH, year to year (Fig. 3c). In the summer, for the period from 01 June to 31 July, mean pH_T was 8.01 ± 0.04, 8.02 ± 0.03, and 8.02 ± 0.03, in 2012, 2013, and 2014, respectively. Likewise, mean diel pH_T cycles changed little from year to year: 0.12 ± 0.08, 0.10 ± 0.03, and 0.10 ± 0.03, for 2012, 2013, and 2014, respectively. These similar summer conditions are notable as mean temperature increased each year in summer: 16.9 ± 0.4°C, 17.6 ± 1.0°C, and 19.0 ± 1.5°C, in 2012, 2013, and 2014, respectively. Summer diel pH cycles were consistently larger than the previous or following winter, from 2012 to 2014, suggesting that the seasonal change in diel pH cycles is consistent interannually and not driven by changes in mean temperature conditions.

Temperature and pH

Throughout the study period, waters warmed seasonally (Fig. 3d–f). SMN was always colder than ALC by ~1 (winter)−4 (summer)°C. PRZ and ALC exhibited similar thermal regimes where temperatures peaked in September and were lowest in March and April (Table 1). As annual warming was evident (e.g., ALC, Fig. 3f), pH and temperature relationships were investigated by month and year.

None of the sites exhibited a significant linear relationship between mean monthly pH and temperature (SMN: $R^2 = 0.28$, $F = 4.1963$, $p = 0.065$, $n = 13$; PRZ: $R^2 = 0.16$, $F = 3.7085$, $p = 0.069$, $n = 22$; ALC: $R^2 = 0.002$, $F = 0.0689$, $p = 0.794$, $n = 39$). Monthly mean pH reached a midpoint maximum over temperature at each site (Fig. 8a). When controlling for variability in pH due to thermal effects, pH_T $_{N16°C}$ did not exhibit a midpoint maximum over temperature (Fig. 8b). Relative to pH_T, pH_T $_{N16°C}$ increased during warm months, following the expected temperature effect of warming on pH. Relative to pH_T, pH_T $_{N16°C}$ remained low during cool months, signifying that low pH at cool temperatures is due to the existing high CO_2 content of the water mass.

When comparing SMN and ALC, low pH events (observations >1 SD below mean pH_T) spanned different temperatures and time frames (Fig. 9). At SMN, low pH_T events, ranging from 7.83 to 8.01, were largely concentrated between 11.5°C and 14°C, and occurred at all hours of the day (Fig. 9a, b). At ALC, low pH_T events ranged from 7.82 to 7.99 under a bimodal distribution of temperatures with a division at 16.5°C (Fig. 9c). At temperatures ≥16.5°C, lowest pH observations occurred during night hours (Fig. 9d). These patterns suggest two different drivers of low pH events: (1) low pH events at cold temperatures (<16.5°C, SMN and ALC) were a function of abiotic processes (e.g., upwelled water) and (2) low pH observations under warm temperatures (≥16.5°C, ALC) were a function of biotic processes
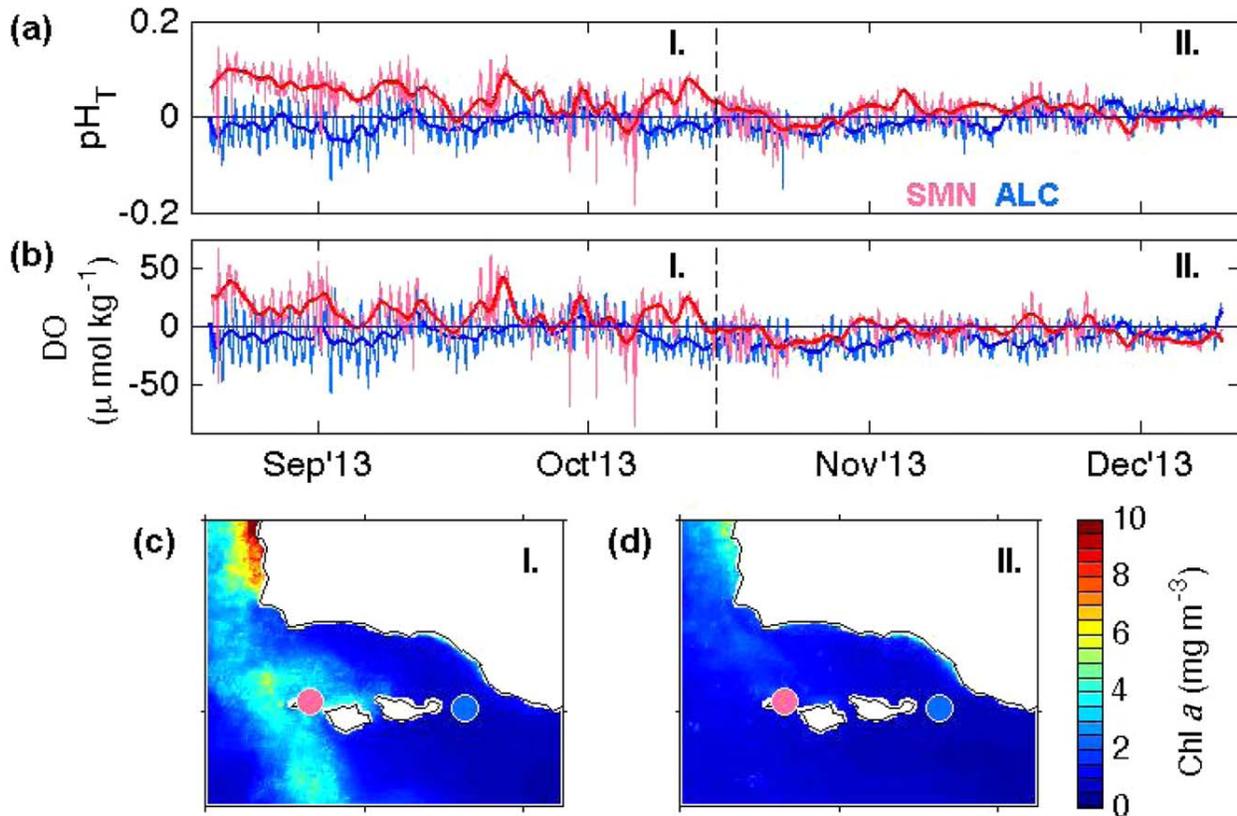
Fig. 5. pH and oxygen anomalies (a, b) at SMN and ALC from August to December and corresponding surface Chl *a* composites during two time periods: Phase I and II. Positive pH and oxygen anomalies (Phase I) were observed at SMN (red) but not at ALC (blue), during a phytoplankton bloom in the western end of the channel (c). Following disappearance of Chl *a* in the channel (Phase II), pH and oxygen returned to nonanomalous conditions at SMN, matching observations at ALC. Bold time-series lines are 48-h low-pass filtered data. Time-series tick marks denote the 1st of the month. Dashed line indicates the start of Phase II. Chl *a* composites represent means for cloud-free pixels using daily satellite images. Map coordinates and site codes are the same as in Fig. 1.

that occurred on a diel cycle (e.g., nighttime ecosystem respiration during warm summer months).

Discussion

In this study, we observed spatial and temporal pH heterogeneity across three sites in a temperate coastal region with persistent abiotic gradients within an EBCS. Each study site was different in terms of habitat and biota with ALC and PRZ representing fixed vegetation (kelp and eelgrass, respectively) and the warmer portion of the SBC, and SMN a more open water site and cooler portion of the SBC. We hypothesized that the persistent temperature, wind, and current gradients across these sites would yield a pH gradient where SMN experiences lower pH than ALC. This hypothesis was not supported due to event-scale pH variability observed across all island sites. For example, while springtime upwelling in 2014 led to a negative pH anomaly at SMN and not at ALC as hypothesized, low pH_T (~7.9) events were observed at PRZ

and ALC in other years. These events occurred during the coldest temperatures, suggesting that seasonal upwelling may, on occasion, influence pH conditions throughout the SBC. All sites experienced event-scale pH increases that correlated with timing of local phytoplankton blooms. Variability in timing and spatial extent of advected upwelled water and phytoplankton blooms, thus, prevented a persistent pH gradient in this region. The pH heterogeneity, described here, reflects a fusion of local and regional drivers and addresses a knowledge gap of how pH dynamics vary over multiple spatial and temporal scales in a coastal region of an EBCS.

We detected various drivers and temporal scales of pH variability (Table 2). One source was diel pH cycles, which differed by (1) site and (2) season. First, the diel pH cycles at PRZ, the eelgrass-dominated site, were nearly double in magnitude, compared to ALC, the kelp forest site. Previous studies observed diel pH cycles of 0.06–0.35 in seagrass beds (Hendriks et al. 2014; Challener et al. 2015) and ~0.1 in kelp forests (Frieder et al. 2012; Krause-Jensen et al. 2015). Second, seasonal
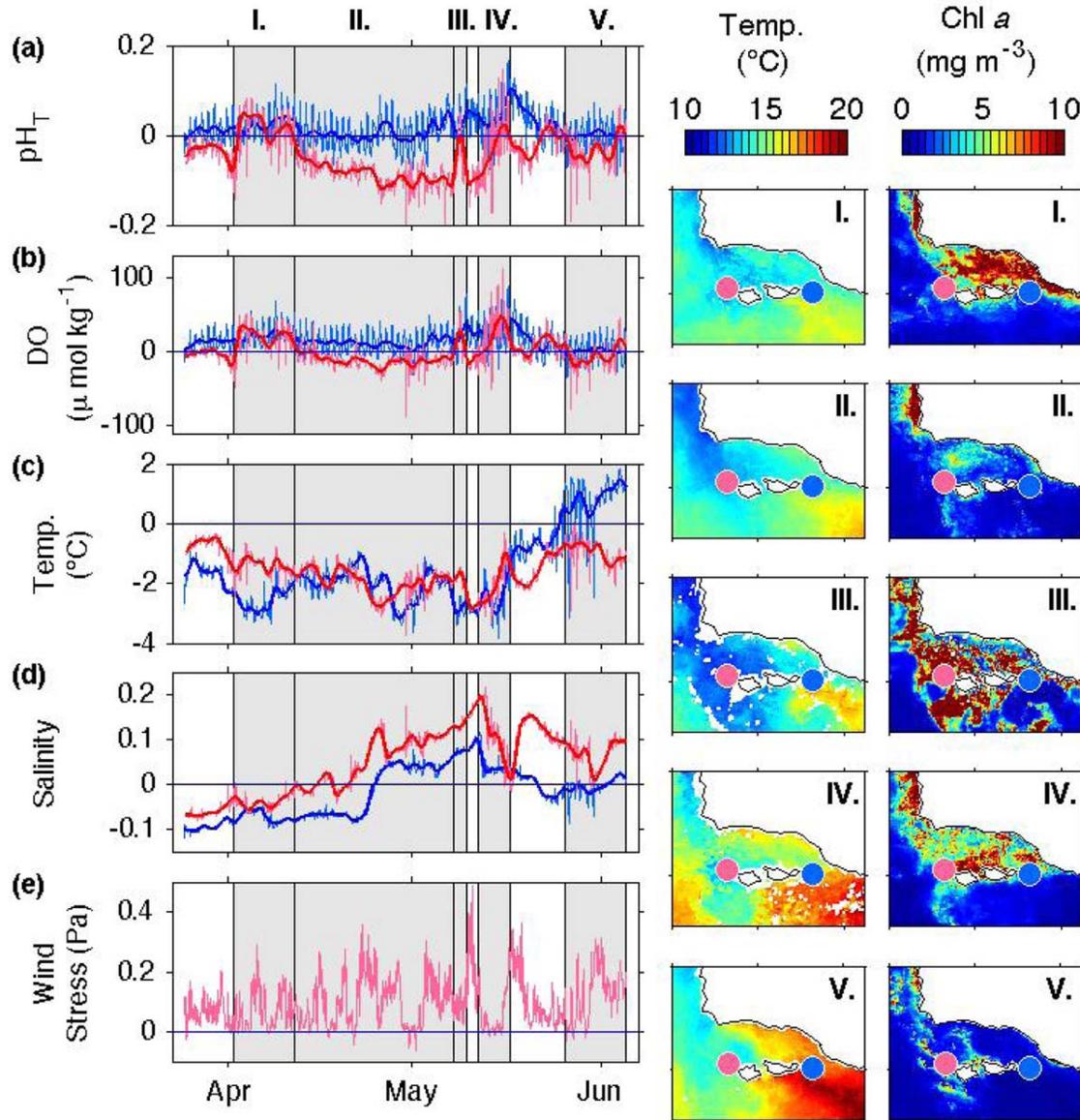
Fig. 6. Changing pH, dissolved oxygen (DO), temperature, and salinity anomalies at SMN (red) compared to ALC (blue) in 2014. Dark lines in time-series represent 48-h low-pass filtered data and tick marks denote the 1st of the month. Wind data are from the National Data Buoy Center station 46054. Transitional phases are numbered with latin numerals. Corresponding sea surface temperature and Chl *a* composites were computed over the time intervals of each phase in gray and represent means for cloud-free pixels using daily satellite images. Map coordinates and site codes are the same as in Fig. 1.

doubling or tripling of diel pH cycles was observed in the kelp forest and eelgrass bed, respectively, and was consistent between years (Fig. 4). Such seasonality in diel pH cycles was also documented in a temperate salt marsh, where diel pH ranges increased more than threefold from winter to summer (Flax Pond, North Atlantic coast, U.S.A., Baumann et al. 2015). In the Southern California Bight, Frieder et al. (2012) found that equatorward currents enhanced diel pH cycles in the La Jolla kelp forest, suggesting that some variability in diel pH cycles may be controlled by water mass movement. Peak diel

pH cycles at SMN matched those of ALC. As SMN is located outside vegetated habitat, changes in diel pH cycles at SMN likely reflect photosynthesis of event-scale phytoplankton blooms. If so, diel pH cycles of 0.1 from blooms could contribute to the observed diel pH cycles at ALC and PRZ.

Moving up in scale from diel cycles, we observed event-scale (days to weeks) changes in pH. During the overlapping period of sensor deployments at SMN and ALC, such events were more prominent at SMN as this site is influenced by equatorward wind stress and currents more so than the other
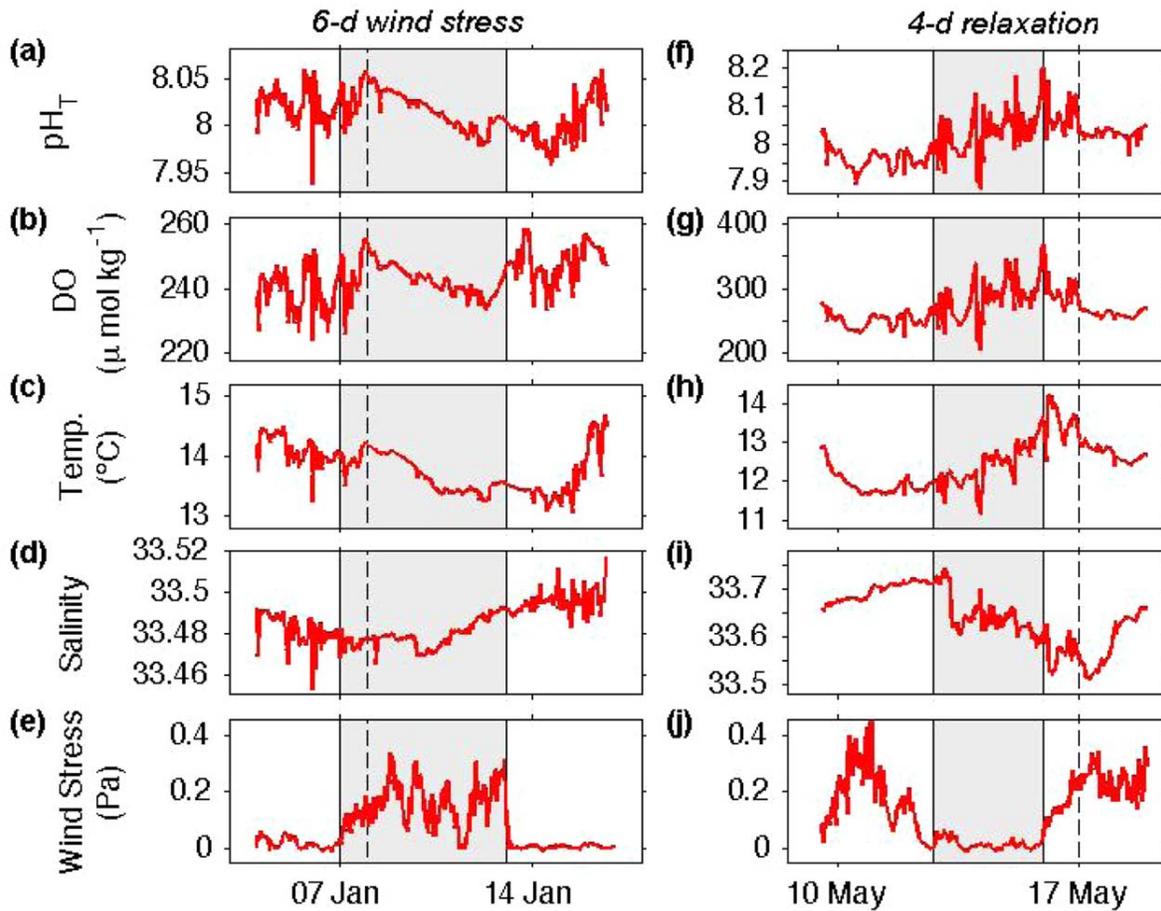
Fig. 7. Wind stress and relaxation event-scale effects on pH, dissolved oxygen (DO), temperature and salinity, at SMN in winter (a–e) and in spring during a phytoplankton bloom (f–j), in 2014. Dashed lines denote the 1-d delay in wind stress effects on high-frequency variability. Scales for *y*-axes are larger for May compared to January observations.

Table 1. Monthly mean (±SD) temperature and pH$_T$ at San Miguel Island (SMN), Santa Cruz Island (PRZ) and Anacapa Island (ALC). Data represent all observations made during this study.

Month	Temperature (°C)			pH$_T$		
	SMN	PRZ	ALC	SMN	PRZ	ALC
1	14.1 ± 0.1	14.2 ± 0.2	14.6 ± 1.3	8.03 ± 0.02	8.00 ± 0.02	8.01 ± 0.04
2	13.3 ± 0.1	14.1 ± 0.2	14.4 ± 1.3	8.05 ± 0.04	7.99 ± 0.04	8.02 ± 0.02
3	13.8 ± 0.0	12.6 ± 0.1	14.1 ± 1.4	8.02 ± 0.01	7.94 ± 0.07	8.01 ± 0.05
4	12.8 ± 0.1	12.7 ± 0.1	14.1 ± 1.1	8.00 ± 0.05	7.94 ± 0.05	8.02 ± 0.04
5	12.9 ± 0.1	14.9 ± 0.2	15.4 ± 0.9	8.00 ± 0.04	8.04 ± 0.06	8.04 ± 0.03
6	14.1 ± 0.1	16.9 ± 0.1	17.4 ± 1.0	8.08 ± 0.04	8.06 ± 0.02	8.02 ± 0.02
7	17.4 ± 0.2	18.6 ± 0.2	18.3 ± 1.4	8.07 ± 0.02	8.03 ± 0.02	8.01 ± 0.02
8	16.1 ± 0.2	16.9 ± 0.1	18.6 ± 1.1	8.08 ± 0.04	8.04 ± 0.03	8.01 ± 0.01
9	14.9 ± 0.1	19.5 ± 0.1	19.7 ± 1.3	8.1 ± 0.02	7.99 ± 0.03	7.99 ± 0.02
10	15.4 ± 0.2	19.2 ± 0.1	19.3 ± 1.2	8.07 ± 0.03	7.98 ± 0.02	7.98 ± 0.02
11	15.5 ± 0.1	17.7 ± 0.1	17.5 ± 1.2	8.07 ± 0.02	8.01 ± 0.02	8.00 ± 0.02
12	14.0 ± 0.1	15.9 ± 0.2	15.8 ± 1.6	8.06 ± 0.02	7.99 ± 0.02	8.00 ± 0.04
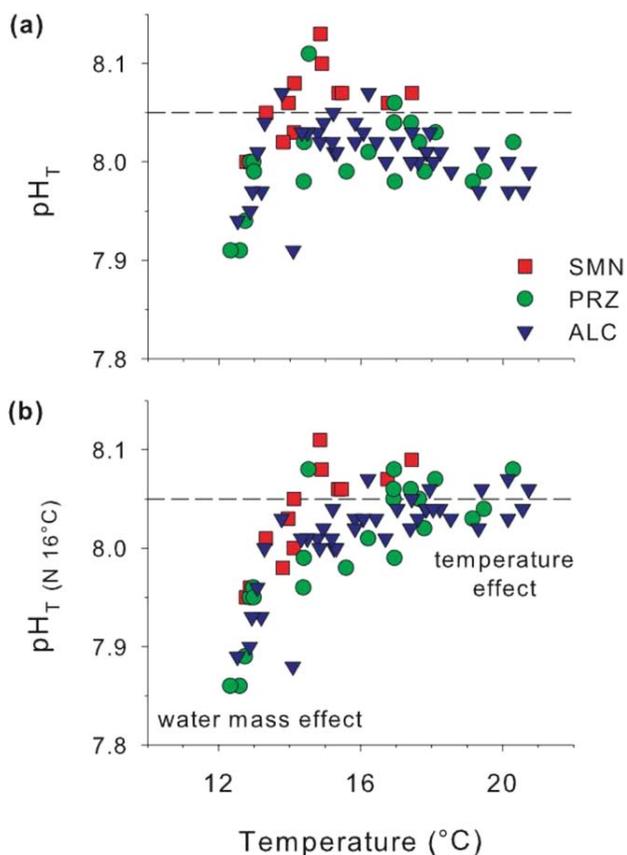
Fig. 8. Scatter plot of monthly mean temperature and pH$_T$ (a) and temperature normalized pH, pH$_{T (N\ 16°C)}$ (b), for SMN (red square), PRZ (green circle), and ALC (blue triangle). As a linear reference, pH$_T$ 8.05 is noted with a dotted line. Site codes are the same as in Fig. 1.

sites (Harms and Winant 1998). SMN exhibited a wider range in pH observations than ALC. We discuss the three observed event-scale pH effects due to (1) upwelling, (2) phytoplankton blooms, and (3) periods of wind relaxation.

First, *upwelling* in the CCS brings low pH (<7.75) seawater onshore (Feely et al. 2008). Outside the SBC and north of Pt. Conception on the mainland, these upwelling events decrease pH$_T$ by 0.3–0.4 (Santa Barbara Coastal LTER unpublished data, Hofmann et al. 2011). As upwelling favorable winds in the CCS would result in downwelling at SMN (a north-facing coastline), the upwelling effects observed at SMN (0.1 pH$_T$ decrease) are likely a signature of low pH, upwelled water masses advected from north of Pt. Conception. The smaller change in pH$_T$ associated with upwelled water at SMN (0.1), compared to north of Pt. Conception (0.3–0.4), suggests a decline in DIC as the water is advected to SMN. This could be due to CO$_2$ off-gassing or uptake of DIC through primary production during transport. The lack of strong upwelling at the islands compared to north of Pt. Conception suggests that the northern Channel Islands

may serve as a spatial refuge from extreme low pH and upwelling events in the future.

Second, *phytoplankton blooms* appeared to increase pH$_T$ by 0.1–0.2 at all island sites. These positive pH anomalies, associated with phytoplankton blooms, yielded spatial differences in pH variability across the islands. For example, a 2-month positive pH anomaly was observed at SMN but not at ALC during a phytoplankton bloom that was localized around San Miguel Island. As SMN is outside of vegetated habitat, observations of increased diel pH cycles during phytoplankton presence suggest that phytoplankton activity contributes to both mean pH and magnitude of diel pH cycles. The spatial differences in pH variability, due to phytoplankton blooms, may be a typical occurrence in the SBC, as phytoplankton blooms occur more frequently in the western portion of the SBC, compared to the eastern end (Otero and Siegel 2004). Channel-wide blooms typically occur in April and May during cold temperatures (Otero and Siegel 2004) and corresponded with positive pH and oxygen anomalies across all sites. Smaller near-shore phytoplankton blooms can occur throughout the year, due to storm runoff (Otero and Siegel 2004), and likely contribute to the spatial variability of event-scale pH anomalies. These event-scale increases in pH may be a feature of pH variability found throughout the Southern California Bight. For example, a 0.1 increase in pH$_T$ was observed in the La Jolla kelp forest during transitions from equatorward to poleward alongshore currents and were attributed to increase ecosystem production, following high-density water intrusion (Frieder et al. 2012).

Third, *periods of wind relaxation* corresponded with an increase in high-frequency (<1 day) pH, oxygen, temperature, and salinity variability. This could stem from physical and biochemical processes disrupted by high wind stress. Wind relaxation and solar heating causes stratification (Mann and Lazier 2005), and propagated internal waves and tides could thus move different water masses across the sensor surface on frequencies <1 d (Booth et al. 2012). Tidal effects on pH have been shown for coastal ecosystems (Frieder et al. 2012; Baumann et al. 2015). Although the pH power spectra in our study showed peaks at 1 and 2 cycles per day (cpd, Supporting Information 4), the peak for 1 cpd was larger than the peak for 2 cpd suggesting that tidal effects were smaller than the effect of biological forcing on pH at our sites, in general. Wind stress causes vertical mixing of the water column (Mann and Lazier 2005) and, in our study, this generally corresponded to high density water intrusion and low high-frequency variability of measured variables (Fig. 7).

Small seasonal trends in pH were observed; pH$_T$ declined from May to October by 0.06 at both ALC and PRZ. During this time, waters warmed 4.3°C and 3.9°C, respectively. Given the increase in monthly mean pH$_T$ $_{N16°C}$ relative to pH$_T$, during warm months, declining summertime pH may largely be driven by thermal effects (i.e., 0.015 pH$_T$ decrease per 1°C increase). Assuming a pH$_T$ decreases 0.015 for every degree
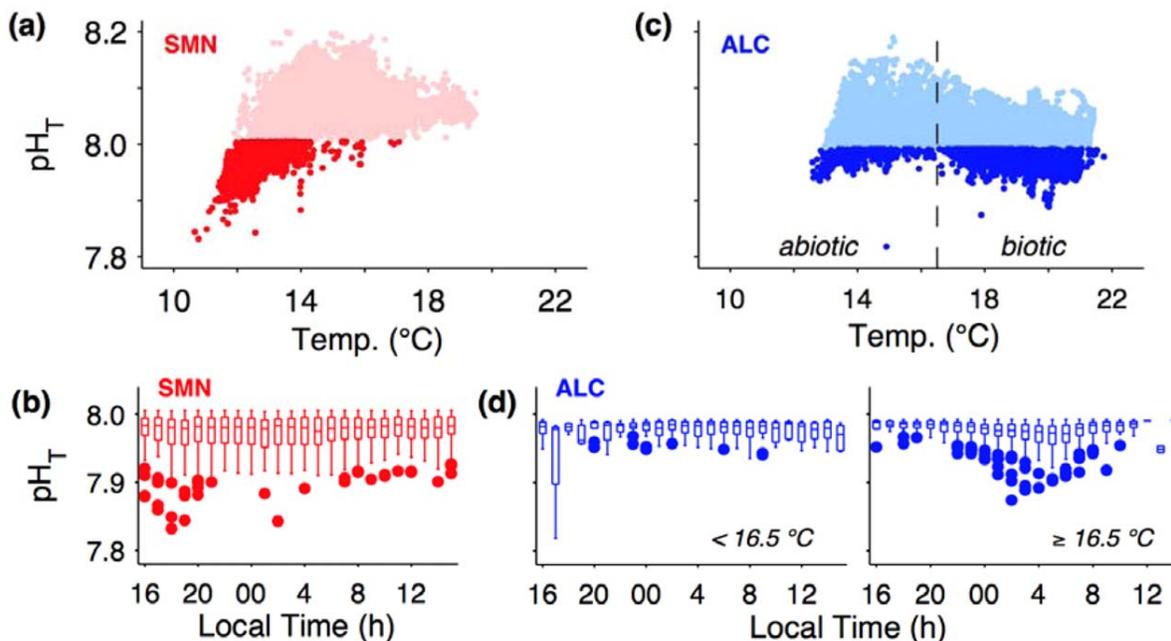
Fig. 9. Observations of pH as a function of temperature at SMN (a) and ALC (c). Darkened dots indicate low pH events (>1 SD below mean pH). Low pH events are displayed by the observed time of day in box plots (b, d). For ALC, box plots of low pH events were divided between <16.5°C or ≥16.5°C, due to the bimodal distribution of low pH events across temperature (c, dashed line). Data were collected on a 30 min sampling frequency from 20 August 2013 to 20 August 2014. Site codes are the same as in Fig. 1.

warming, expected pH decline, due to warming alone, would be 0.06 and matches the observed seasonal change in pH. CO_2 off gassing, primary production and increased ecosystem respiration under warming may also contribute to seasonal changes in pH. As poleward advection of southern waters increases in fall and contributes to seasonal warming in the SBC (Lynn and Simpson 1987; Otero and Siegel 2004), the observed seasonal pH cycle at PRZ and ALC may represent a pattern present throughout the Southern California Bight. For example, a similar seasonal decrease in pH_T (<0.1) was also observed in Santa Monica Bay, ~60 km east of the Channel Islands (Leinweber and Gruber 2013), and predicted in model simulations (0.04) of near-shore seasonal pH variability in the southern portion of the CCS (Hauri et al. 2013). In the southern region of the CCS, the timing of seasonal primary production (pH increase) counteracts seasonal warming (pH decrease), resulting in an overall small seasonal pH cycle compared to the northern portion of the CCS (Hauri et al. 2013). Larger seasonal pH change has been documented in other coastal regions. For example, pH_{NBS} declined by 0.6 from early spring to late summer in Flax Pond, a temperate salt marsh (Baumann et al. 2015). In Flax Pond, lowest pH was observed in August and correlated with maximum diel pH cycles. As such, the 0.6 seasonal change in pH was attributed to seasonal changes in community production and respiration that were influenced by seasonal warming and increases in day

length (Baumann et al. 2015). This was not the case at our sites because diel pH cycles at ALC and PRZ peaked during different seasons (Fig. 4), supporting the conclusion that the small summertime decline in pH in our study region is likely due to seasonal warming (Hauri et al. 2013).

While our dataset has gaps, we were able to gain some inferences on pH over an interannual time frame (Fig. 3). Stable pH conditions were observed each year in summer at ALC, despite increasing temperatures. Late winter and spring appear to be the most variable in terms of pH events, making predictions of future pH challenging for this portion of

Table 2. Summary of temporal pH change associated with different processes. Ocean acidification is referenced for comparison. Bold indicates a biotic effect. + *hf* stands for increased high-frequency variability.

Time scale	Variable	Effect on pH	ΔpH_T
Centennial	Ocean acidification	−	0.42*
Seasonal	Warming (4°C)	−	0.06
Event	Advection of upwelled water	−	0.1–0.15
	Phytoplankton blooms	+	0.1–0.2
	Wind relaxation	+ *hf*	< 0.1
Daily	**Photosynthesis/respiration**	±	0.05–0.2

*End century prediction, RCP8.5 climate scenario (Pörtner et al. 2014).

the year. Using the approach from Keller et al. (2014), we can estimate how long the pH time-series needs to be at the Channel Islands before detecting an ocean acidification trend. This time of emergence (ToE) is defined as "the point in time when the trend signal ($S \times$ ToE) exceeds two times the background variability (N)," where S is the ocean acidification trend (Keller et al. 2014):

$$\text{ToE} = (2 \times N)/S \qquad (2)$$

For our estimate of ToE, we used data from ALC, which exhibited an overall pH SD of 0.04 (= N), despite occasional low pH events. Assuming a constant -0.002 yr^{-1} change in pH$_T$ (= S) for the North Pacific (Dore et al. 2009; Ishii et al. 2011), ToE for detecting the anthropogenic signal at Anacapa Island would be 40 yr and more than triple the length of time estimated to detect ocean acidification trends in the open ocean (Keller et al. 2014). Coastal acidification rates, however, may be much faster (e.g., -0.058 yr^{-1} at Tatoosh Island, Washington, U.S.A., Wootton and Pfister 2012) and so trends may be detectable sooner.

Application to future research strategies

Incorporating environmental realism into laboratory experiments remains a vital research goal and challenge within ocean change biology (Mcelhany and Busch 2013; Reum et al. 2015; Takeshita et al. 2015). Here, the scarcity of time-series data from coastal marine ecosystems can be a major resource gap for the research community. Such data provide present-day exposures of resident biota necessary to study pH tolerance and adaptive capacity. Here, we show that the northern Channel Islands is a location within an EBCS that experiences relatively mild effects of coastal upwelling and strong biological influences within vegetated habitats. These findings have two implications for the sensitivity of local biota to ocean acidification in this region: (1) the northern Channel Islands may provide a *spatial refuge* from extreme low pH (<7.7, sensu Feely et al. 2008), associated with upwelling and (2) pH increase due to primary production may provide a *temporal refuge* from ocean acidification, in the future. Identifying the effects of spatio-temporal pH variability on organisms and ecosystems remains an underexplored area of research. Evidence is emerging that such patterns can result in selection for tolerant genotypes (e.g., Kelly et al. 2013) and may manifest in transgenerational effects (Murray et al. 2014; Parker et al. 2015; Thor and Dupont 2015).

We emphasize the importance of addressing multistressor scenarios in future research endeavors. It is known that pH, temperature and oxygen stress co-occurs or changes seasonally in coastal habitats (Baumann et al. 2015; Reum et al. 2015). In this study, comparison of low pH events (driven by abiotic and biotic processes) across sites revealed unique combinations of pH and temperature stress that may be relevant on an organismal scale (Fig. 9). A similar perspective was gleaned from a coral reef ecosystem in Australia where anomalous pH and thermal stress were found to be asynchronous in time (Kline et al. 2015). Understanding the biological and physiological importance of environmental exposures over different temporal scales and various combinations is therefore critical. Simple warming and acidification treatments in laboratory experiments may not be relevant if those conditions are not reflective of realistic future exposures across a species range (Reum et al. 2015).

We recommend designing experiments that are (1) finetuned to local habitat conditions to which the experimental organisms are inherently acclimatized and (2) carefully designed to address biological responses on specific temporal scales (e.g., diel, seasonal, etc.). Reum et al. (2015) provide suggestions for experimental design based on habitat conditions of CO_2 and temperature for upwelling systems, and Bockmon et al. (2013) have developed a laboratory infrastructure to conduct multistressor experiments. pH exposures for coastal organisms cannot be assumed, and studies of biology should ideally be coupled with environmental data such as those presented here.

References

Barton, A., B. Hales, G. G. Waldbusser, C. Langdon, and R. A. Feely. 2012. The Pacific oyster, *Crassostrea gigas*, shows negative correlation to naturally elevated carbon dioxide levels: Implications for near-term ocean acidification effects. Limnol. Oceanogr. **57**: 698–710. doi:10.4319/lo.2012.57.3.0698

Baumann, H., R. B. Wallace, T. Tagliaferri, and C. J. Gobler. 2015. Large natural pH, CO_2 and O_2 fluctuations in a temperate tidal salt marsh on diel, seasonal, and interannual time scales. Estuaries Coast. **38**: 220–231. doi:10.1007/s12237-014-9800-y

Bednaršek, N., R. A. Feely, J. C. P. Reum, B. Peterson, J. Menkel, S. R. Alin, and B. Hales. 2014. *Limacina helicina* shell dissolution as an indicator of declining habitat suitability owing to ocean acidification in the California Current Ecosystem. Proc. R. Soc. Lond. B Biol. Sci. **281**: 20140123. doi:10.1098/rspb.2014.0123

Bockmon, E. E., C. A. Frieder, M. O. Navarro, L. A. White-Kershek, and A. G. Dickson. 2013. Technical note: Controlled experimental aquarium system for multi-stressor investigation of carbonate chemistry, oxygen saturation, and temperature. Biogeosciences **10**: 5967–5975. doi:10.5194/bg-10-5967-2013

Booth, J. A. T., and others. 2012. Natural intrusions of hypoxic, low pH water into nearshore marine environments on the California coast. Cont. Shelf Res. **45**: 108–115. doi:10.1016/j.csr.2012.06.009

Bresnahan, P. J., T. R. Martz, Y. Takeshita, K. S. Johnson, and M. Lashomb. 2014. Best practices for autonomous measurement of seawater pH with the Honeywell Durafet. Methods Oceangr. **9**: 44–60. doi:10.1016/j.mio.2014.08.003

Challener, R. C., L. L. Robbins, and J. B. Mcclintock. 2015. Variability of the carbonate chemistry in a shallow, seagrass-dominated ecosystem: Implications for ocean acidification experiments. Mar. Freshw. Res. doi:10.1071/MF14219

Dickson, A. G., and F. J. Millero. 1987. A comparison of the equilibrium constants for the dissociation of carbonic acid in seawater media. Deep-Sea Res. I **34**: 1733–1743. doi:10.1016/0198-0149(87)90021-5

Dickson, A. G., C. L. Sabine, and J. R. Christian. 2007. Guide to best practices for ocean CO_2 measurements, v. 3, 191 p. PICES Special Publication.

Dong, C., E. Y. Idica, and J. C. Mcwilliams. 2009. Circulation and multiple-scale variability in the Southern California Bight. Prog. Oceanogr. **82**: 168–190. doi:10.1016/j.pocean.2009.07.005

Dore, J. E., R. Lukas, D. W. Sadler, M. J. Church, and D. M. Karl. 2009. Physical and biogeochemical modulation of ocean acidification in the central North Pacific. Proc. Natl. Acad. Sci. U.S.A. **106**: 12235–12240. doi:10.1073/pnas.0906044106

Dorman, C., and C. Winant. 2000. The structure and variability of the marine atmosphere around the Santa Barbara Channel. Mon. Weather Rev. **128**: 261–282. doi:10.1175/1520-0493(2000)128<0261:TSAVOT>2.0.CO;2

Feely, R. A., C. L. Sabine, J. M. Hernandez-Ayon, D. Ianson, and B. Hales. 2008. Evidence for upwelling of corrosive "acidified" water onto the continental shelf. Science **320**: 1490–1492. doi:10.1126/science.1155676

Frieder, C. A., S. H. Nam, T. R. Martz, and L. A. Levin. 2012. High temporal and spatial variability of dissolved oxygen and pH in a nearshore California kelp forest. Biogeosciences **9**: 3917–3930. doi:10.5194/bg-9-3917-2012

Frieder, C. A., J. P. Gonzalez, E. E. Bockmon, M. O. Navarro, and L. A. Levin. 2014. Can variable pH and low oxygen moderate ocean acidification outcomes for mussel larvae? Glob. Chang. Biol. **20**: 754–764. doi:10.1111/gcb.12485

García, H. E., and L. I. Gordon. 1992. Oxygen solubility in seawater: Better fitting equations. Limnol. Oceanogr. **37**: 1307–1312. doi:10.4319/lo.1992.37.6.1307

Gruber, N., C. Hauri, Z. Lachkar, D. Loher, T. L. Frölicher, and G.-K. Plattner. 2012. Rapid progression of ocean acidification in the California Current System. Science **337**: 220–223. doi:10.1126/science.1216773

Hales, B., T. Takahashi, and L. Bandstra. 2005. Atmospheric CO_2 uptake by a coastal upwelling system. Global Biogeochem. Cycles **19**, GB1009, doi:10.1029/2004GB002295

Harms, S., and C. D. Winant. 1998. Characteristic patterns of the circulation in the Santa Barbara Channel. J. Geophys. Res. **103**: 3041–3065. doi:10.1029/97JC02393

Hauri, C., and others. 2013. Spatiotemporal variability and long-term trends of ocean acidification in the California Current System. Biogeosciences **10**: 193–216. doi:10.5194/bg-10-193-2013

Hendriks, I. E., and others. 2014. Photosynthetic activity buffers ocean acidification in seagrass meadows. Biogeosciences **11**: 333–346. doi:10.5194/bg-11-333-2014

Hoegh-Guldberg, O., and others. 2014. The Ocean, p. 1655–1731. *In* V. R. Barros, and others [eds.], Climate change 2014: Impacts, adaptation, and vulnerability. Part B: regional aspects. Contribution of working group II to the fifth assessment report of the intergovernmental panel on climate change. Cambridge Univ. Press.

Hofmann, G. E., and others. 2011. High-frequency dynamics of ocean pH: A multi-ecosystem comparison. PLoS One **6**: e28983. doi:10.1371/journal.pone.0028983

Hofmann, G. E., and others. 2014. Exploring local adaptation and the ocean acidification seascape—studies in the California Current Large Marine Ecosystem. Biogeosciences **11**: 1053–1064. doi:10.5194/bg-11-1053-2014

Iles, A. C., T. C. Gouhier, B. A. Menge, J. S. Stewart, A. J. Haupt, and M. C. Lynch. 2012. Climate-driven trends and ecological implications of event-scale upwelling in the California Current System. Glob. Chang. Biol. **18**: 783–796. doi:10.1111/j.1365-2486.2011.02567.x

Ishii, M., N. Kosugi, D. Sasano, S. Saito, T. Midorikawa, and H. Y. Inoue. 2011. Ocean acidification off the south coast of Japan: A result from time series observations of CO_2 parameters from 1994 to 2008. J. Geophys. Res. **116**: C06022. doi:10.1029/2010JC006831

Kahru, M., R. M. Kudela, M. Manzano-Sarabia, and B. G. Mitchell. 2012. Trends in the surface chlorophyll of the California Current: Merging data from multiple ocean color satellites. Deep Sea Res. Part II: Top. Stud. Oceanogr. **77**: 89–98. doi:10.1016/j.dsr2.2012.04.007

Kapsenberg, L., and G. E. Hofmann. 2014. Signals of resilience to ocean change: High thermal tolerance of early stage Antarctic sea urchins (*Sterechinus neumayeri*) reared under present-day and future pCO_2 and temperature. Polar Biol. **37**: 967–980. doi:10.1007/s00300-014-1494-x

Kapsenberg, L., A. L. Kelley, E. C. Shaw, T. R. Martz, and G. E. Hofmann. 2015. Near-shore Antarctic pH variability has implications for biological adaptation to ocean acidification. Sci. Rep. **5**: 9638. doi:10.1038/srep10497

Keller, K., F. Joos, and C. Raible. 2014. Time of emergence of trends in ocean biogeochemistry. Biogeosciences **11**: 3647–3659. doi:10.5194/bg-11-3647-2014

Kelly, M. W., J. L. Padilla-Gamiño, and G. E. Hofmann. 2013. Natural variation and the capacity to adapt to ocean acidification in the keystone sea urchin *Strongylocentrotus purpuratus*. Glob. Chang. Biol. **19**: 2536–2546. doi:10.1111/gcb.12251

Kline, D. I., and others. 2015. Six month *in situ* high-resolution carbonate chemistry and temperature study on a coral reef flat reveals asynchronous pH and temperature anomalies. PLoS One **10**: e0127648. doi:10.1371/journal.pone.0127648

Krause-Jensen, D., C. M. Duarte, I. E. Hendriks, L. Meire, M. E. Blicher, N. Marbà, and M. K. Sejr. 2015. Macroalgae

contribute to nested mosaics of pH variability in a sub-Arctic fjord. Biogeosciences **12**: 4895–4911. doi:10.5194/bg-12-4895-2015

Lagerloef, G. S., and R. L. Bernstein. 1988. Empirical orthogonal function analysis of advanced very high resolution radiometer surface temperature patterns in Santa Barbara Channel. J. Geophys. Res. **93**: 6863–6873. doi:10.1029/JC093iC06p06863

Lee, K., and others. 2006. Global relationships of total alkalinity with salinity and temperature in surface waters of the world's oceans. Geophys. Res. Lett. **33**: L19605. doi:10.1029/2006GL027207

Leinweber, A., and N. Gruber. 2013. Variability and trends of ocean acidification in the Southern California Current System: A time series from Santa Monica Bay. J. Geophys. Res. **118**: 3622–3633. doi:10.1002/jgrc.20259

Liu, X., M. C. Patsavas, and R. H. Byrne. 2011. Purification and characterization of meta-cresol purple for spectrophotometric seawater pH measurements. Environ. Sci. Technol. **45**: 4862–4868. doi:10.1021/es200665d

Lynn, R. J., and J. J. Simpson. 1987. The California Current System: The seasonal variability of its physical characteristics. J. Geophys. Res. **92**: 947–912. doi:10.1029/JC092iC12p12947

Malvezzi, A. J., and others. 2015. A quantitative genetic approach to assess the evolutionary potential of a coastal marine fish to ocean acidification. Evol. Appl. **8**: 352–362. doi:10.1111/eva.12248

Mann, K. H., and J. R. N. Lazier. 2005. Vertical structure in coastal waters: Coastal upwelling regions, p. 165–215. *In* Dynamics of marine ecosystems, 3rd ed. Blackwell Publishing Ltd, Malden, MA USA. doi: 10.1002/9781118687901.ch5

Martz, T. R., J. G. Connery, and K. S. Johnson. 2010. Testing the Honeywell Durafet® for seawater pH applications. Limnol. Oceanogr.: Methods **8**: 172–184. doi:10.4319/lom.2010.8.172

Mcelhany, P., and D. S. Busch. 2013. Appropriate pCO_2 treatments in ocean acidification experiments. Mar. Biol. **160**: 1807–1812. doi:10.1007/s00227-012-2052-0

Mehrbach, C., C. H. Culberso, J. E. Hawley, and R. M. Pytkowic. 1973. Measurement of apparent dissociation constants of carbonic acid in seawater at atmospheric pressure. Limnol. Oceanogr. **18**: 897–907. doi:10.4319/lo.1973.18.6.0897

Murray, C. S., A. Malvezzi, C. J. Gobler, and H. Baumann. 2014. Offspring sensitivity to ocean acidification changes seasonally in a coastal marine fish. Mar. Ecol. Prog. Ser. **504**: 1–11. doi:10.3354/meps10791

Otero, M. P., and D. Siegel. 2004. Spatial and temporal characteristics of sediment plumes and phytoplankton blooms in the Santa Barbara Channel. Deep Sea Res. Part II: Top. Stud. Oceanogr. **51**: 1129–1149. doi:10.1016/S0967-0645(04)00104-3

Parker, L. M., W. A. O'connor, D. A. Raftos, H.-O. Pörtner, and P. M. Ross. 2015. Persistence of positive carryover effects in the oyster, *Saccostrea glomerata*, following transgenerational exposure to ocean acidification. PLoS One **10**: e0132276. doi:10.1371/journal.pone.0132276

Pespeni, M. H., and others. 2013. Evolutionary change during experimental ocean acidification. Proc. Natl. Acad. Sci. **110**: 6937–6942. doi:10.1073/pnas.1220673110

Pörtner, H.-O., and others. 2014. Ocean systems, p. 411–484. *In* C. B. Field, and others [eds.], Climate change 2014: Impacts, adaptation, and vulnerability. Part A: Global and sectoral aspects. Contribution of working group II to the fifth assessment report of the intergovernmental panel on climate change. Cambridge Univ. Press.

Price, N. N., T. R. Martz, R. E. Brainard, and J. E. Smith. 2012. Diel variability in seawater pH relates to calcification and benthic community structure on coral reefs. PLoS One **7**: e43843. doi:10.1371/journal.pone.0043843

Reum, J. C. P., and others. 2015. Interpretation and design of ocean acidification experiments in upwelling systems in the context of carbonate chemistry co-variation with temperature and oxygen. ICES J. Mar. Sci. doi:10.1093/icesjms/fsu231

Robbins, L. L., M. E. Hansen, J. A. Kleypas, and S. C. Meylan. 2010. CO2calc—A user-friendly seawater carbon calculator for Windows, Max OS X, and iOS (iPhone). U.S. Geological Survey Open-File Report 2010–1280.

Selkoe, K. A., S. D. Gaines, J. E. Caselle, and R. R. Warner. 2006. Current shifts and kin aggregation explain genetic patchiness in fish recruits. Ecology **87**: 3082–3094. doi:10.1890/0012-9658(2006)87[3082:CSAKAE]2.0.CO;2

Sydeman, W. J., M. Garcia-Reyes, D. S. Schoeman, R. R. Rykaczewski, S. A. Thompson, B. A. Black, and S. J. Bograd. 2014. Climate change and wind intensification in coastal upwelling ecosystems. Science **345**: 77–80. doi:10.1126/science.1251635

Takeshita, Y., and others. 2015. Including high frequency variability in coastal ocean acidification projections. Biogeosciences **12**: 5853–5870. doi:10.5194/bg-12-5853-2015

Thor, P., and S. Dupont. 2015. Transgenerational effects alleviate severe fecundity loss during ocean acidification in a ubiquitous planktonic copepod. Glob. Chang. Biol. **21**: 2261–2271. doi:10.1111/gcb.12815

van Heuven, S., D. Pierrot, J. W. B. Rae, E. Lewis, and D. W. R. Wallace. 2011. MATLAB program developed for CO_2 system calculations. ORNL/CDIAC-105b. Carbon Dioxide Information Analysis Center, Oak Ridge National Laboratory, U.S. Department of Energy. doi:10.3334/CDIAC/otg.CO2SYS_MATLAB_v1.1

Wang, D., T. C. Gouhier, B. A. Menge, and A. R. Ganguly. 2015. Intensification and spatial homogenization of coastal upwelling under climate change. Nature **518**: 390–394. doi:10.1038/nature14235

Wetzel, R. G., and G. E. Likens. 1991. Limnological analyses, 2nd ed. Springer-Verlag.

Wootton, J. T., and C. A. Pfister. 2012. Carbon system measurements and potential climatic drivers at a site of rapidly

declining ocean pH. PLoS One **7**: e53396. doi:10.1371/
journal.pone.0053396

Yu, P. C., P. G. Matson, T. R. Martz, and G. E. Hofmann.
2011. The ocean acidification seascape and its relationship
to the performance of calcifying marine invertebrates:
Laboratory experiments on the development of urchin
larvae framed by environmentally-relevant pCO_2/pH. J.
Exp. Mar. Biol. Ecol. **400**: 288–295. doi:10.1016/
j.jembe.2011.02.016